[6]Reddy, N. M., Nagashetty, K., Jagadeesh, G., and Reddy, K. P. J., "Review of Hypersonic Research Investigations in IISc Shock Tunnel (HST-1)," *Sadhana*, Vol. 21, Pt. 6, 1996, pp. 741–773.

[7]Jagadeesh, G., Reddy, N. M., Nagashetty, K., and Reddy, K. P. J., "Forebody Convective Heat Transfer Measurements over Large-Angle Blunt Cones at Hypersonic Mach Number," AIAA Paper 98-2601, June 1998.

[8]Cheng, K. K., Hall, J. G., Golian, T. C., and Hertzberg, A., "Boundary-Layer Displacement and Leading-Edge Bluntness Effects in High Temperature Hypersonic Flow," *Journal of the Aerospace Sciences*, Vol. 28, No. 5, 1961, pp. 353–381.

T. C. Lin
Associate Editor

Aeromaneuvering in the Martian Atmosphere: Simulation-Based Analyses

Roy S. Smith*
University of California, Santa Barbara, Santa Barbara, California 93106
Kenneth D. Mease†
University of California, Irvine, Irvine, California 92697
and
David S. Bayard‡ and David L. Farless§
Jet Propulsion Laboratory, California Institute of Technology, Pasadena, California 91109

Introduction

THE science requirements of future Mars missions include increasing accuracy in the specification of the landing site. In situ science or sample return missions from small craters or ancient lake beds considered to be prime sites for potential exobiology, require a 3-σ target accuracy of 10 km or less.[1] Controlled atmospheric aeromaneuvering will be used to decelerate the vehicle and to guide it to a prespecified terminal point above the surface. At that point a parachute will be deployed to further decelerate the vehicle. An engine will be used for the final controlled descent, from approximately 5 km to the surface.

This Note describes a simulation environment developed to study the guidance, navigation, and control (GNC) aspects of the aeromaneuvering phase. The simulation is modular and based on the widely used MATLAB®/SIMULINK® environment, making it easily upgraded or applied to other landing problems, including landing on other planets or small bodies. A more detailed, and more mission specific, Mars landing simulation is described by Streipe et al.[2] The simulation environment described here is suitable for developing GNC algorithms, investigating the impact of the approach navigation, and performing technology tradeoff studies.

Simulation Environment

The simulation uses a modular approach with each major aspect of the complete system dynamics handled by a separate module. This allows the different aspects of the problem to be developed, upgraded, and modified relatively independently of each other. The major program modules, and conceptual links between each, are illustrated in Fig. 1.

The estimation, guidance, and control aspects have been implemented in separate modules, conforming to historical practice in spacecraft control work. In this problem it is evident that a closer integration of these aspects has the potential for significant performance improvement, and this could be relatively easily done in our simulation.

The environment and spacecraft models are accessed through common modules where flags are used to specify the choice of model, for example, geocentric or geodetic planet models, or even alternative planets. The code for the environment and spacecraft models is linked separately into each module in which it is used. Separate flags are maintained for the simulated physical system models and the GNC models so that effects of knowledge errors may be investigated.

Entry Dynamics

The entry dynamics model used has been derived from the work of Etkin,[3] using the assumption of a rotating planet with its center fixed in inertial space. The vehicle state includes a full six-degree-of-freedom model plus a variable mass (see Ref. 4 for details).

Vehicle Characteristics

Any vehicle model supplying the aerodynamic coefficients, mass properties, and actuator configuration in the correct format can be accomodated. The current vehicle model is based on the Pathfinder entry vehicle (see Refs. 5 and 6 for physical details) augmented with attitude control thrusters and a c.m. offset to generate a lift vector. Eight thrusters are used in the current spacecraft module giving decoupled roll, pitch, and yaw moments.

The aerodynamic model takes into account the effect of the c.m. offset on the pitch and yaw dynamics and allows different nominal lift/drag ratio (L/D) vehicles to be simulated easily. Boussalis[7] describes a longitudinal aerodynamic model, developed from Newtonian impact dynamics, and this forms the basis of the model used in the simulation. The L/D relationship, as a function of angle of attack α is close to linear and can be reasonably approximated by $L/D = -0.0129\alpha$ deg. At $|\alpha| > 20$ deg, the unprotected rear of the vehicle is exposed. Considering $\alpha = -18$ deg as the limit gives a maximum L/D of 0.23.

The roll, pitch, and yaw moment coefficients, C_l, C_m, and C_n, respectively, are modeled by $C_l = 0$, $C_m = C_{\text{moz}} dZ + C_{\text{ma}}\alpha + C_{\text{mq}} q$, and $C_n = -C_{\text{ma}}\beta + C_{\text{nr}} r$, where β is the sideslip angle and q and r are the pitch and yaw rates, respectively. For a nonzero value of the z-axis c.m. offset dZ a nonzero trim value for α (denoted here by α_0) is given by $\alpha_0 = -C_{\text{moz}}/C_{\text{ma}}\, dZ$.

Environmental Models

Atmospheric forces dominate the entry, making the aerodynamic and atmospheric density models more important than the gravity model. In this case a simple spherical planet gravity model is used, $g = \mu/R^2$ m/s^2, where R is the distance from the planet center. Both spherical and geodetic[8] models are available for target and location definition.

The Mars atmospheric density ρ is modeled in exponential form $\rho = \rho_r e^{-\beta(h - h_r)}$, where ρ_r is the reference density $\rho_r = 7.8 \times 10^{-4}$ kg/m^3, specified at an altitude of $h_r = 31.800 \times 10^3$ m. The inverse of the scale height is denoted by β and has a value of $\beta = 10^{-4}$ m^{-1}. A percentage error can be applied to the density to evaluate the effects of density variations on the control system. The modular nature of the simulation environment makes it possible to incorporate a higher fidelity model, for example, Mars Global Reference Atmospheric Model (MarsGRAM) at a later date.

Guidance and Control

The simulation environment supports switching between different guidance algorithms. The focus of the guidance research has been on drag-based predictive tracking algorithms, and two such algorithms (from Refs. 9 and 10) are currently implemented in the simulation.

Drag-tracking algorithms are based on the observation that the predicted range to go is given by integrating a drag/energy profile.

Received 2 April 1999; revision received 6 September 1999; accepted for publication 4 October 1999.

*Associate Professor, Electrical and Computer Engineering. Senior Member AIAA.

†Professor, Mechanical and Aerospace Engineering. Associate Fellow AIAA.

‡Senior Technical Staff, Autonomy and Control. Member AIAA.

§Member Technical Staff, Navigation and Flight Mechanics.

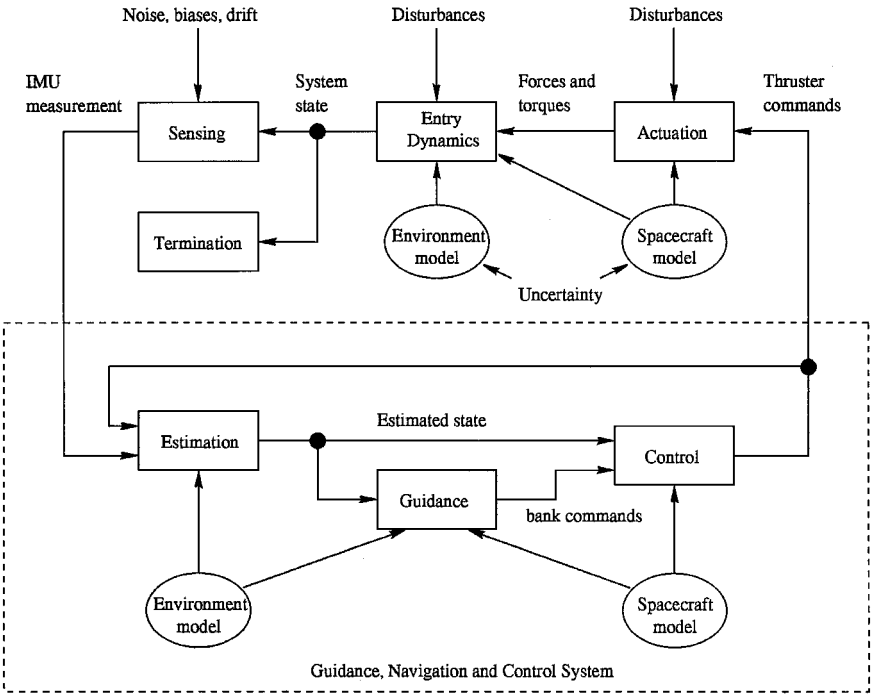

Fig. 1 Conceptual arrangement of the simulation modules, showing the division between the simulated physical system and the GNC system.

Nominal entry and atmospheric conditions are used to develop a nominal drag profile. A periodic (20-s) drag profile update is performed to adjust the drag profile to null the predicted terminal point errors resulting from entry and atmospheric uncertainty.

A drag-tracking loop, actuated via the bank angle, uses a discrete-time proportional-integral-derivative (PID) controller with feedback linearization[11] and gain scheduling, operating at a frequency of 0.1 Hz. Side-to-side modulation of the bank angle gives control over the cross-range error.

An attitude controller maneuvers the spacecraft via the pitch, roll, and yaw thrusters to achieve the specified bank angle. It has a secondary objective of minimizing the off-nominal deviations in α and β to maintain the actual L/D as close as possible to that assumed in the guidance law. The guidance algorithm leads to two distinct operational modes in the attitude controller: bank reversals and bank angle tracking. Bank reversals typically switch the lift vector from one side to the other with large transitions, and the attitude controller uses a bang–bang switching approach to slew the bank angle in an approximately time-optimal fashion.

Landing Analyses

Several Mars landing issues are studied with the simulation environment. These are not exhaustive studies and do not take the place of extensive Monte Carlo analyses, but they do illustrate the utility of the simulation environment for initial trade studies and closed-loop aeromaneuvering system design.

Lift/Drag Ratio Actuation Study

The variable c.m. offset aerodynamic model gives the ability to assess the control authority as a function of L/D, without developing high-fidelity aerodynamic models for different vehicle configurations. This trade study gives a first-order measure of the actuation authority.

Figure 2 shows the achievable ground footprints for L/D values of $L/D = 0.23$, 0.15, and 0.08 (corresponding to $\alpha = -18$, -12, and -6 deg), with the axes centered at the ballistic trajectory target point that is 202.7 km south and 639.2 km west of the atmospheric entry point at latitude 22.984° north, longitude 338.904° east. The entry conditions are velocity 7.35 km/s, flight-path angle -14.2 deg, and heading angle 253.1 deg.

The actuation authority drops dramatically as a function of L/D. The maximum range extent for the $L/D = 0.23$ case is 1054 km.

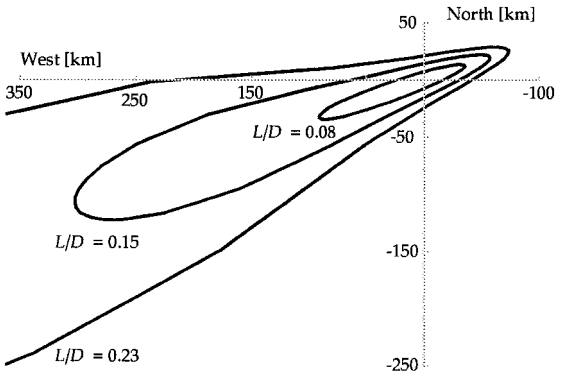

Fig. 2 Open-loop actuation authority for several *L/D*.

This drops to 383 km for $L/D = 0.15$ and further to 134 km for $L/D = 0.08$. These values represent the maximum possible control authority and are only achieved if a fixed bank angle is held throughout the entry.

Atmospheric Entry Navigation Knowledge Errors

Knowledge errors are critical to achievable performance because, in the base configuration at least, there is no direct position measurement available to the estimation and control system. Integrating acceleration and velocity measurements from the inertial measurement unit (IMU) gives an estimate of the position relative to the entry point. Uncertainty in the entry point is propagated throughout the duration of the flight. An atmospheric density estimator and a more detailed atmosphere model may be able to reduce the errors from those shown here.

Horizontal knowledge errors, arising from arrival time and azimuth angle knowledge errors, cannot be corrected unless there is a beacon or other planet relative position information available. The azimuth errors have only a small cross-range effect on the error ellipse. Uncertainty in the knowledge of the arrival time will have a potentially large effect on the downrange error (for trajectories that are predominately east–west). This is not studied in detail here, but it is simple to work out from the rotation of the planet and the timing knowledge error.

Knowledge errors in the velocity vector direction are estimated to be 0.1 deg. For comparative purposes a knowledge error of 0.05 deg

Table 1 Entry knowledge error landing ellipses[a]

Trajectory type	Entry error, deg	−40% density	−25% density	Nominal density	+25% density	+40% density
Lifting	0.1	16.6 × 1.5	15.5 × 1.5	14.5 × 1.4	13.7 × 1.4	13.3 × 1.4
Ballistic	0.1	7.1 × 1.1	6.8 × 1.0	6.3 × 1.0	6.0 × 1.0	5.9 × 1.0
Lifting	0.05	8.3 × 0.8	7.8 × 0.7	7.2 × 0.7	6.8 × 0.7	6.7 × 0.7
Ballistic	0.05	3.6 × 0.5	3.4 × 0.5	3.2 × 0.5	3.0 × 0.5	3.0 × 0.5

[a]Semimajor × semiminor axes in kilometers.

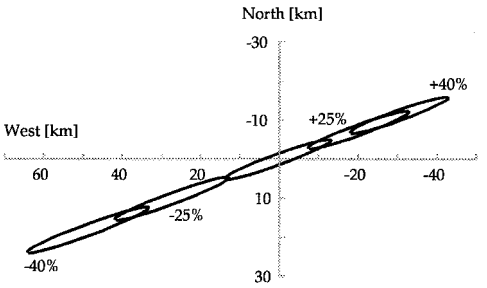

a) Lifting trajectory

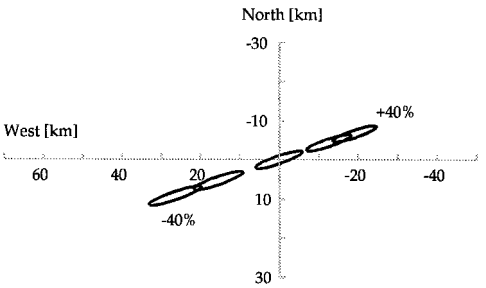

b) Ballistic trajectory

Fig. 3 Error footprints for a 0.1-deg entry knowledge error.

is also considered. The effects of the knowledge errors are estimated by propagating the error to the planet surface under a variety of atmospheric uncertainty assumptions. The errors in the nominal endpoint that arise purely from the atmospheric uncertainty are measurable and, to a large extent, correctable, by the estimator/controller. Therefore, it is the size of the error ellipses, rather than their position on the planet, that gives an estimate of the effect of the knowledge error. Figure 3 illustrates the 0.1-deg knowledge error footprint for atmospheric density variations of −40, −25, 0, +25, and +40% with respect to nominal for lifting ($L/D = 0.17$) and ballistic trajectories. The axes are centered at the nominal target in each case.

The ballistic trajectory shows smaller ellipses and less of an effect due to atmospheric uncertainty, illustrating that the effect of the knowledge error is strongly influenced by both the vehicle L/D and the design of the entry path. Table 1 details the error ellipse sizes and includes a 0.05-deg knowledge error study for comparison. The ultimate objective is to have a total aeromaneuvering error ellipse with a semimajor axis less than 10 km. The knowledge error ellipse alone is larger than this, suggesting that a lower knowledge error at the entry point may be necessary.

Nominal Entry: Mars Surveyor Program 2001 Landing

The simulation facility has been used in support of the Mars Surveyor Program 2001 Landing. The final tuning has been performed on the simulation facility described by Streipe et al.[2] The Mars 2001 Landing atmospheric entry conditions considered here are latitude 17.247° north, longitude 254.123° east; velocity 6.97 km/s, flight-path angle −14.5 deg, heading angle 100.8 deg, and altitude 125.0 km. The nominal $L/D = 0.12$ ($\alpha = -9.3$ deg). The target was chosen as the midpoint between two ±nominal bank angle open-loop trajectories and the terminal error in this case was 2.9 km.

Figure 4 shows the commanded and actual bank angles during the aeromaneuvering entry. The peak dynamic pressure and maximum

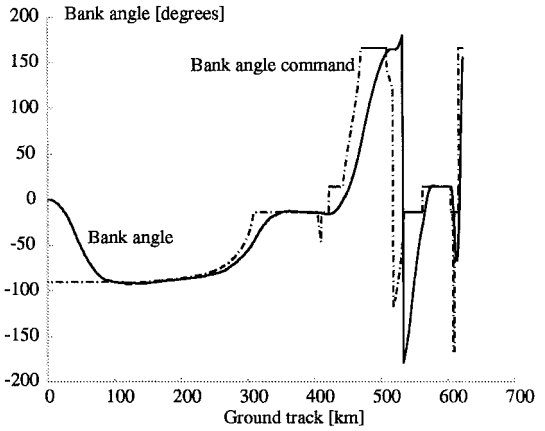

Fig. 4 Nominal closed-loop trajectory, commanded and actual bank angle.

control authority occur around 300 km. The bank angle command illustrates periods of drag tracking, as well as bank angle sign switches for azimuth control. The control actuation limitations are evident in the actual bank angle.

Conclusions

A MATLAB/SIMULINK-based simulation for Mars precision landings has been developed. The modular nature of the simulation environment makes it readily adaptable to other landing problems and allows for straightforward enhancement of the underlying models. It has been used for L/D actuation authority and entry condition knowledge error tradeoff studies, as well as the development of closed-loop guidance and control algorithms in support of the Mars Surveyor Program 2001 Landing mission.

Acknowledgments

This research is supported through the Mars Exploration Technology Program at the Jet Propulsion Laboratory (JPL), California Institute of Technology, under contract with NASA. R. Smith is supported by JPL under Contract 699381, and K. Mease is supported by JPL under Contract 9609609. The authors acknowledge the contributions by other members of the JPL Mars Precision Landing technology development team, A. Ahmed, S. Ploen, M. Munir, and K.-Y. Tu, and discussions with the Mars Surveyor Program 2001 Mission Atmospheric Flight Team, led by R. Braun, NASA Langley Research Center.

References

[1]Braun, R. D., Spencer, D. A., Carpenter, J. R., and Willcockson, W. H., "Mars Precision Landing," 49th International Astronautical Congress, Paper IAF98-Q.3.03, Sept.–Oct. 1998.

[2]Streipe, S. A., Queen, E. M., Powell, R. W., Braun, R. D., Cheatwood, F. M., Aguirre, J. T., Sachi, L. A., and Lyons, D. T., "An Atmospheric Guidance Algorithm Testbed for the Mars Surveyor Program 2001 Orbiter and Lander," AIAA Paper 98-4569, Aug. 1998.

[3]Etkin, B., *Dynamics of Atmospheric Flight*, 1st ed., Wiley, New York, 1972, pp. 121–195.

[4]Smith, R. S., Bayard, D. S., and Mease, K. D., "Mars Precision Landing; an Integrated Estimation, Guidance and Control Simulation," Center for Control Engineering and Computation, TR CCEC-98-0918, Univ. of California, Santa Barbara, CA, Sept. 1998.

[5]Spencer, D. A., and Braun, R. D., "Mars Pathfinder Atmospheric Entry Trajectory Design," American Astronomical Society, Paper 95-379, San

Diego, CA, Aug. 1995.

[6]Braun, R. D., Powell, R. W., Engelund, W. C., Gnoffo, P. A., Weilmuenster, K. J., and Mitcheltree, R. A., "Six-Degree-of-Freedom Atmospheric Entry Analysis for the Mars Pathfinder Mission," AIAA Paper 95-0456, Jan. 1995.

[7]Boussalis, D., "Investigation of the Longitudinal Motion of Low-lift Entry Vehicles," Jet Propulsion Lab., TR EM 3456-96-002, California Inst. of Technology, Pasadena, CA, May 1996.

[8]Sofair, I., "Improved Method for Calculating Exact Geodetic Latitude and Altitude," *Journal of Guidance, Control, and Dynamics*, Vol. 20, No. 4, 1997, pp. 824–826.

[9]Tu, K.-Y., Munir, M., Mease, K., and Bayard, D., "Drag-Based Predictive Tracking Guidance for Mars Precision Landing," AIAA Paper 98-4573, Aug. 1998.

[10]Munir, M., "Entry Guidance Law for a Low Lift/Drag Mars Precision Landing," M.S. Thesis, Dept. of Mechanical and Aerospace Engineering, Univ. of California, Irvine, CA, 1997.

[11]Mease, K. D., and Kremer, J.-P., "Shuttle Entry Guidance Revisited Using Nonlinear Geometric Methods," *Journal of Guidance, Control, and Dynamics*, Vol. 17, No. 6, 1994, pp. 1350–1356.

C. A. Kluever
Associate Editor

Thermal and Structural Test Results for a Venus Deep-Atmosphere Instrument Enclosure

Jeffery L. Hall,* Paul D. MacNeal,† Moktar A. Salama,‡ Jack A. Jones,§ and Matthew Kuperus Heun¶
Jet Propulsion Laboratory, California Institute of Technology, Pasadena, California 91109-8099

Nomenclature

a, b = curve-fit constants
T = temperature, °C
T_{ref} = curve-fit reference temperature, °C
κ = thermal conductivity, W/m-K
κ_0 = thermal conductivity at reference temperature, W/m-K

Introduction

In situ exploration of the surface and deep atmosphere of Venus is impeded by an environment that is hostile to scientific instruments. Temperature, pressure, and corrosion protection must be provided to ensure survival of instruments and electronics for even short durations. Previous missions to Venus, namely the Soviet Venera landers and the U.S. Pioneer-Venus atmospheric probes, used a combination of titanium pressure vessels and thermal insulation for this purpose.[1,2] Recent work has investigated the possibility of using a balloon to deliver a small payload into the deep atmosphere of Venus for surface imaging and atmospheric investigations.[3–6] However, smaller payloads suffer from reduced volume-to-surface-area ratios and therefore heat up more quickly. This disadvantage has motivated the development of more efficient thermal insulation that retains the simplicity of design and operational robustness needed in the current era of smaller and cheaper space missions. The solution of using vacuum multilayer insulation (MLI) was originally suggested in the context of a novel Venus balloon mission concept capable of multiple descents into the hot lower atmosphere.[7] However, concerns about the efficiency of MLI on small spherical enclosures with multiple penetrations and the difficulty of ensuring the necessary high vacuum under Venus atmospheric pressure and temperature conditions led to a more robust alternative idea using fiberglass insulation with the void space filled with low thermal conductivity xenon gas. The present work investigated the performance of this xenon-filled fiberglass insulation in conjunction with a new, low thermal conductivity internal structure. A full-scale prototype was constructed and tested at simulated Venus surface temperature and pressure conditions. Also, a centrifuge test was performed to verify the ability of the structure to tolerate the expected deceleration load upon entry into the Venusian atmosphere. The details of the design and the test results are presented herein.

Prototype Design and Construction

The prototype design was guided by the mission specification of protecting 15 kg of payload at Venus surface conditions of 460°C and 9.2×10^6 Pa (92 atm) pressure. Optimal performance of the camera and other electronic components requires a near-Earthlike state, namely 10^5 Pa pressure and 20°C temperature. To meet the mission requirement of 1-h residence time near the surface of Venus, it was necessary to limit the heat flow to the payload to less than 100 W. The other key design driver was the need to survive typical deceleration loads when the probe enters the Venusian atmosphere from space. A nominal value of 250 g was selected for the prototype design based on the Pioneer-Venus experience[1,2] and current mission studies.[6]

The prototype is based on a concentric sphere design in which the payload is located within the inside sphere and thermal insulation is located in the annulus between the spheres. An expanded view of the enclosure is shown in Fig. 1, and a list of component masses is presented in Table 1. The spherical shape was selected because it results in the lightest structure per unit volume for withstanding external buckling loads, a fact that led to its use on the earlier Pioneer-Venus probes. As with those earlier probes, titanium alloy Ti-6Al-4V was selected for the outer sphere because of its excellent strength-to-weight ratio and its ability to tolerate the sulfuric acid found in the clouds of Venus. The nominal diameter is 38 cm, and the shell thickness is 0.38 cm, giving a diameter-to-thickness ratio of 100. Given an expected buckling failure mode, this shell has a computed 1.3 pressure safety factor at 460°C. For comparison, the Pioneer-Venus probes used a slightly less conservative design for which the diameter-to-thickness ratio ranged from 116 to 136 (Ref. 1).

The inside sphere is 30 cm in diameter with a wall thickness of 0.76 mm and is constructed from Type-304 stainless steel. The structure used to connect to the inside and outside spheres consists of three sets of rigid Ti-6Al-4V struts. The first is a single, thin-walled conical structure rigidly connected to the spheres at their south poles. This aperture cone is welded to the outer sphere and has a flange onto which the inside sphere is bolted. It is inside of this aperture cone that the camera window would be located in a fully functional probe. The second part is an array of six thin-walled Ti-6Al-4V struts arranged around the aperture cone. These six struts are welded to the outer sphere but have a nominal 0.5 mm gap at the inside sphere

Table 1 Mass list for prototype

Component	Mass, kg
Outer sphere	10.9
Inner sphere	4.2
Simulated payload	15.6
Fiberglass insulation	1.4
Miscellaneous	1.5
Total	33.6

Received 15 January 1999; revision received 6 August 1999; accepted for publication 20 August 1999.

*Staff Engineer, Advanced Thermal and Structural Technology Group, 4800 Oak Grove Drive. Senior Member AIAA.

†Senior Engineer, Instrument Structures and Dynamics Group, 4800 Oak Grove Drive. Member AIAA.

‡Principal Engineer, Instrument Structures and Dynamics Group, 4800 Oak Grove Drive. Associate Fellow AIAA.

§Principal Engineer, Advanced Thermal and Structural Technology Group, 4800 Oak Grove Drive. Senior Member AIAA.

¶Staff Engineer; currently Staff Engineer, Global Aerospace Corporation, P.O. Box 93305, Pasadena, CA 91109-3305.